ISSN 2231-3478 (Print)
JUSPS-B Vol. 31(2), 8-16 (2019). Periodicity-Monthly
Section B
(Online) ISSN 2319-8052

JOURNAL OF ULTRA SCIENTIST OF PHYSICAL SCIENCES
An International Open Free Access Peer Reviewed Research Journal of Physical Sciences
website:- www.ultrascientist.org
Estd. 1989

# Synthesis and Spectroscopic Studies of $Gd_2Zr_2O_7$ Oxides

S SRIJITH*[1], V T KAVITHA[2] and K MANIAMMAL[3]

[1]Research and Post graduate Department of Physics, SN College Kollam,
[2]Research and Post graduate Department of Mahatma Gandhi College, Thiruvananthapuram,
[3]Research and Post graduate Department of Physics, University of Kerala, Kariavattom
Corresponding author:srijithkeanu@gmail.com
http://dx.doi.org/10.22147/jusps-B/310201

**Acceptance Date 19th February, 2019, Online Publication Date 28th February, 2019**

**Abstract**

Nano-ceramics have received a considerable attention during the last two decades due to their capability to demonstrate improved or unique characteristics as compared to conventional bulk ceramic materials. $Gd_2Zr_2O_7$ powders, synthesised by Solution combustion synthesis, were investigated in detail for the defect fluorite-pyrochlore phase transition behaviour below 1500°C. Our Xrd and Raman analyses clearly reveal the structural phase transition in this system. X-ray diffraction data analyses confirm that there is a defect fluorite structure in $Gd_2Zr_2O_7$ , having cubic lattice. The rearrangement in anionic sublattice in this system during structural phase transition from the Pyrochlore phase to disordered fluorite results in the shift in Pyrochlore-related peak. Band gap energy of the sample was obtained from UV-Visible spectroscopic analysis of the sample. It was found to be 4.82 eV.

*Key words :* Defect fluorite, Solution Combustion Synthesis. Rietveld analysis, Raman spectra, Bandgap.

## 1. Introduction

The Pyrochlore-type $Gd_2Zr_2O_7$ is a kind of $A_2B_2O_7$ oxides which has the smallest value of radius ratio of cations, 1.46. $Gd_2Zr_2O_7$ is one of the most interesting pyrochlores because oxygen conductivity increases with the degree of lattice disorder[1]. One of the prolific features of Pyrochlore- type $Gd_2Zr_2O_7$ is its structural flexibility and compositional diversity, which allows a wide range of entered elements. Its structure and degree of order in the binary system can be tuned by changing the stoichiometry and temperature[2,3]. The Pyrochlore-

type to Fluorite-type phase transition temperature for $Gd_2Zr_2O_7$ is about 1550 °C. Recently, it was found that $Gd_2Zr_2O_7$ and other pyrochlore oxides are radiation-resistant ceramics that disorder to a defect fluorite structure that does not become amorphous[5].

Among the ternary metallic oxides, compounds of the general formula, $A_2B_2O_7$ (A and B are metals), represent a family of phases isostructural to the mineral pyrochlore, (NaCa)(NbTa)O6F/(OH) [2,4]. The space group of the ideal pyrochlore structure is Fd3m and there are eight molecules per unit cell (Z=8). In $A_2B_2O_7$ pyrochlores, A is usually a trivalent rare earth ion, but can also be a mono, divalent cation and B may be 3d, 4d or 5d transition element having an appropriate oxidation state required for charge balance to give rise to the composition $A_2B_2O_7$ [6]. Pyrochlore unit cell contains eight $A_2B_2O(1)_6O(2)$ formula units, and for better and easy understanding one-eighth of the pyrochlore unit cell is shown in Fig.1.1. (b). With the choice of B atom as origin, the cation sublattice is an alternate arrangement of A-site (16*d*) and B-site (16*c*) cations along the 110 direction in an fcc lattice. The anion sublattice is comprised of three different oxygen sites, two of which are occupied (8*b*) and (48*f*), and the third site (8*a*) is vacant. Hence, the anion vacancies are ordered. The A-site cations are eight coordinated and are located within scalenohedra (distorted cubes). The B-site cations are six-coordinated and are located within trigonal antiprisms. All anion sites are tetrahedrally coordinated: the 8*a* site is surrounded by four B cations, and the 8*b* site by four A cations. The 48*f* oxygen is surrounded by two A and two B cations that are slightly displaced from the center of the tetrahedral site towards the unoccupied 8*a* site. The magnitude of the displacement is represented by the positional parameter, *x*, of oxygen at the 48*f* site, which is 0.375 for the ideal fluorite structure. The pyrochlore crystal structure also tolerates vacancies at the A and O sites to a certain extent with the result that cation and anion migration within the solid is feasible. Recently, it has been shown by our group that anion rich pyrochlores like $Ce_2Zr_2O_8$ are also possible[7]. The pyrochlore structure is closely related to the fluorite structure $AX_2$, except that there are two cation sites and one-eighth of the anions are absent as shown in the Fig.1.1 (a) for the ordered pyrochlore, $A_2B_2O_7$, the phase stability of the superstructure is basically determined by the A and B site cation radius ratio.

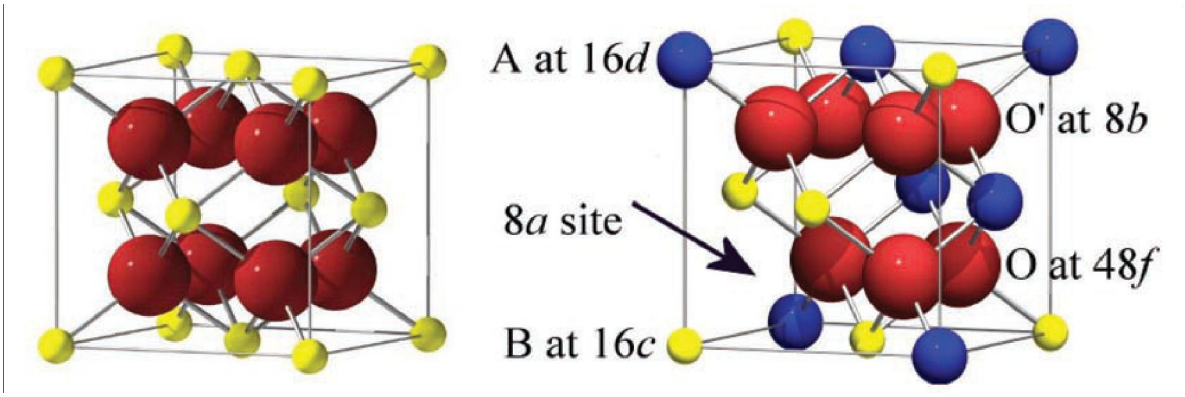


Fig.1.1 (a): Unit cell of fluorite (Fmm), yellow atoms represent $A^{4+}$ cations and the red $O^{2-}$.
Fig.1.1 (b): Unit cell of pyrochlore (Fd3m), Blue spheres represent $A^{3+}$ cations, yellow $B^{4+}$ and red $O^{2--}$

The electrical properties of the pyrochlores vary from highly insulating through semiconducting to metallic behaviour. It has been reported that few rare-earth Molybdate and Ruthenate pyrochlores show semiconductor to metal transition. Pyrochlores like $Cd_2Re_2O_7$ exhibit superconductivity at lower temperature.

The system where the A and B ions are in the maximum possible oxidation states, exhibits excellent dielectric properties. The electrical properties of the pyrochlores having Bi ion, like $Bi_2Ru_2O_7$, are interesting, because the lone pair of electron on Bi contributes to the electrical property of the compound. Many of the pyrochlores like $La_2Zr_2O_7$ act as thermal barrier coating whereas some other systems like $Y_2Sn_2O_7$ act as excellent host matrices for photoluminescence. Oxide ion conduction is also possible in pyrochlores if the compositions are tuned properly[7]. High pressure response of pyrochlore is also worth mentioning. Mostly researchers have found that pyrochlores transform to fluorite phase or some other phases at higher pressure. In addition, pyrochlores are excellent host matrices for nuclear waste immobilization because it can dissolve various lanthanides, actinides and other elements which are generated from nuclear reactors. Heavy ion irradiation of pyrochlore oxides leads to the distortion of the unit cell and the order-disorder transition occurs during the relaxation and recovery phase of the damage cascade. The energy deposited due to irradiation can be dissipated by swapping the A and B cations and the structure transforms to defect fluorite form. However, in case of pyrochlores having large difference in ionic radii of A and B cations cannot exchange their sites. Therefore, these pyrochlores amorphize under high irradiation dose to dissipate the extra energy[8]. Hence, $Gd_2Zr_2O_7$ was chosen as a suitable host material for fixation of some of the nuclear waste products. It has been found that stability of the pyrochlores under radiation environment increases with decrease in radius ratio. This can be explained on the basis of antisite defect formation. In this paper, we fabricated and investigated $Gd_2Zr_2O_7$ oxides through solution combustion synthesis (SCS) and study their structural pattern.

## 2. Experimental set up

Among the available, solution chemistry routes, the solution combustion techniques are capable of producing the nanocrystalline powders of oxide ceramics at a lower calcination temperature in a surprisingly short time[9-12]. Generally the powder obtained by this technique has compositional homogeneity, the highest degree of phase purity coupled with the improved powder characteristics like narrow particle size distribution, higher surface area and better sinterability. The very high exothermicity generated during combustion manifests in the form of either flame or fire and hence, the process is termed as auto-ignition process. The basic characteristics of the fuel are that it should be able to maintain the compositional homogeneity among the constituents and get combusted with an oxidizer at a low ignition temperature. A considerable number of parameters such as type of fuel, fuel to oxidizer ratio, combustion temperature and amount of water can affect the reaction and products of the SCS method[13].

A mixture of high purity Gd $(NO_3)_3.6H_2O$ (2.8542 g), Zr O $(NO_3)_2$ $2H_2O$ (2.1458 g) and citric acid (7.3618 gm) are taken in a beaker. After mixing the metal nitrate solutions in a beaker, 30 ml nitric acid is added and stirred continuously for 30 minutes. The fuel used for the synthesis is citric acid. In order to attain a pH of 7, liquor ammonia is added drop by drop and the solution is heated at 100 ºC to remove as much of water content. After evaporation of the water content, the slurry was then introduced into a muffle furnace preheated to 300°C.The mixture frothed and ignited to combust with a flame, giving a voluminous and foamy $Gd_2Zr_2O_7$. The as prepared powder is annealed at 1000 ºC for 3 hrs. The theoretical equation assuming complete combustion can be written as follows:

$$2\,Gd(NO_3)_3.6H_2O + 2\,Zr\,O(NO_3)_2.6H_2O + 11C_6H_8O_7 \rightarrow Gd_2Zr_2O_7 + 66\,CO_2$$

## 3. Results and discussion

*3.1 Phase characterization by Xrd :*

The structure and phase purity of the powder were examined by XRD using Regaku, DMax C, Japan X-ray diffractometer with Nickel filtered Cu $K_\alpha$radiation. The XRD pattern of the as prepared powder sample obtained by the present combustion synthesis is shown in figure.3.1.1

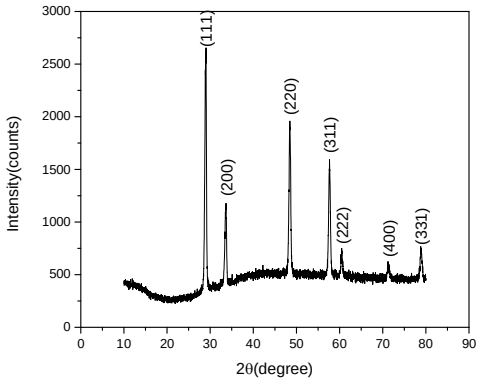


Figure.3.1.1 XRD pattern of $Gd_2Zr_2O_7$

The powder XRD patterns of the sample confirm that the sample is crystalline in nature. Also, the diffraction peak is slightly broadened indicating small crystallite size. All the XRD peaks are indexed according to the defect fluorite-type unit cell with the *Fd*3*m* space group. As Pyrochlore is a superstructure of a fluorite-like array of atoms, its diffraction pattern consists of a set of strong intensities representative of the average fluorite structure plus an additional set of superstructure intensities. The superstructure peaks at $2\theta$ *at* $\approx 14^o$, $38^o$, $46^o$, etc. are very weak in intensity[14, 15]. The intensities of superstructure diffraction maxima depend on a combination of factors, such as the degree of ordering, difference in the average scattering factors of the elements involved, and the distribution of oxygen vacancies (16). Progressive structural transformation into defect Pyrochlore structure can also lead to a decrease in intensity of the superstructure peaks. Hence it is very difficult to directly determine from the XRD pattern whether the average structure of the compounds is defect Pyrochlore or defect fluorite. From the absence of the superstructure peaks, it can be concluded that the structure is defect fluorite[17]. All the reflections in the Xrd pattern shows that $Gd_2Zr_2O_7$ has cubic lattice, with lattice parameter a = 10.503 Å. Figure 3.2 shows examples of the refinement fitting using the Rietveld method for the $Gd_2Zr_2O_7$ annealed at 1000 °C for 3 h. As a starting model, all the Gd ions are assigned to the 16d sites and, correspondingly, the Zr ions in the 16c site. When annealed at temperatures 1000 °C, only the disordered fluorite structure type is retained due to the mixed occupancy of metal cations at the large eight-coordinated 16c site and the smaller six-coordinated 16d site. All of the structural refinement results are summarized in Table 3.1.1. However, the significantly greater scattering from cations in the 16d site, as evidenced in the diffraction pattern, suggests partial occupancy of Gd ions on the 16d sites. Because of the coupled exchange, Zr must also occupy the 16c site. However, refinement of the XRD pattern at 1000°C based on this assumption results in a negative occupancy of Zr on the 16c sites, which may suggest that Gd and the Zr remained at the 16d and 16c sites respectively.

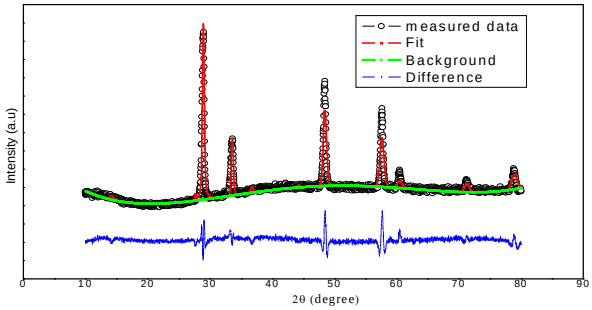


Figure 3.1.2 Refinement fitting using the Rietveld method for the $Gd_2Zr_2O_7$

Table: 3.1.1 XRD Reûnement Results of the Structural Parameters and Grain Size As Measured by XRD for $Gd_2Zr_2O_7$

| crystal structures: pyrochlore Fd3m (S.P. 227) | |
|---|---|
| | treatment T (°C)/ time (h) : 1000/3 |
| unit cell, a (nm) | 10.5030 |
| Gd in 16d (0.5,0.5,0.5), Occ | 1.0000 |
| Zr in 16c (0,0,0), Occ | 1.0000 |
| O in 48f | |
| ($X_{48f}$,0.125,0.125),Occ | 0.9755 |
| O in 8b(0.375,0.375,0.375), Occ | 0.8964 |
| $X_{48f}$ | 0.3467 |
| Rw | 0.0611 |
| $R_{wp}$ | 0.0811 |
| $\chi^2$ | 3.118 |
| grain size calculated from XRD (nm) | 26 |

*3.2 Determination of Average Crystallite Size Using Scherrer equation :*

Crystallite size is a measure of the size of a coherently diffracting domain. Due to the presence of polycrystalline aggregates, crystallite size is not generally the same thing as particle size. Scherrer equation is the simplest method of determining the average crystallite size of a nanocrystalline sample from X-ray diffraction line broadening,

$$t = K\lambda / (\beta_{hkl})_{measured} \times Cos\theta_{hkl}$$

A Pseudo-Voigt 1 function which assumes the peak shape is symmetrical was used to fit the peak profiles. Pseudo-Voigt 1 is one of the most convenient functions used for the profile fitting of X-ray diffraction peaks and it is represented by the expression.

$$y = y_0 + A\left[\frac{2\omega}{\pi\left(x - x_c\right)^2 + \omega^2} + \frac{\left(1-\mu\right)\sqrt{4\ln 2}\left(e^{-\frac{4\ln 2\left(x-x_c\right)^2}{\omega}}\right)}{\sqrt{\pi}\omega}\right] \quad (1)$$

The curve fitting was done using Microcal Origin Version 8. The best fit was chosen taking into account the minimum error as well as the realistic values for individual variables. Figure 3.2.1 shows examples of the curve fitting using the pseudo Voigh 1 function. From Table 3.2.1, it can be noted that the average crystallite size of the sample is ~26 nm.

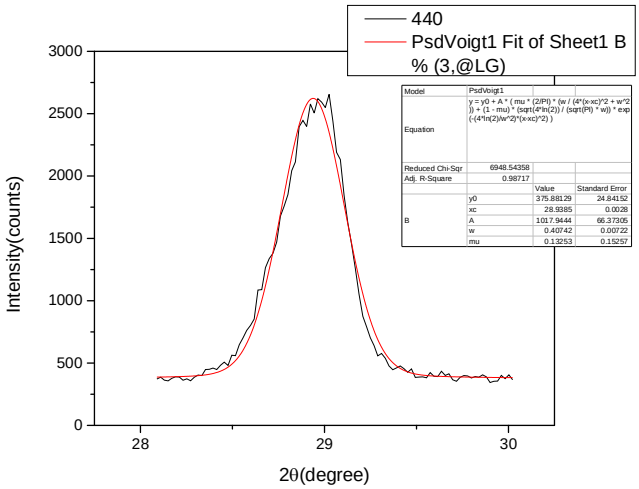


Fig: 3.2.1 Peak fitting using pseudo Voigh 1 function

Table 3.2.1: Scherrer size of crystallites

| Compound | Structure | XRD (2Θ) | Particle Size (nm) D=(0.9*1.540598)/(β cos Θ) | | |
|---|---|---|---|---|---|
| | | | FWHM (β) | COS Θ | D (Å) |
| $Gd_2Zr_2O_7$ | Defect Fluorite | 29.0399 | 0.40702 | 0.968 | 189.050 |
| | | 33.7039 | 0.3542 | 0.957 | 214.775 |
| | | 48.3656 | 0.12 | 0.912 | 604.291 |
| | | 57.7048 | 0.432 | 0.876 | 161.172 |
| | | 60.5123 | 0.24 | 0.864 | 286.111 |
| | | 71.179 | 0.336 | 0.813 | 192.413 |
| | | 78.8674 | 0.336 | 0.773 | 182.759 |

*3.3 Raman spectroscopic analysis :*

X-ray diffraction is more sensitive to disorder in the cation sublattice than the anion sublattice since the X-ray scattering power of oxygen is much less than rare-earth (as well as transition metal) cations. However, Raman spectroscopy is very sensitive to metal–oxygen vibrational modes rather than metal–metal vibrational modes. Therefore, Raman spectroscopy is an excellent tool to analyse the extent of disorder in pyrochlores and hence to distinguish between pyrochlore-type phases and defect fluorite type phases. The FT-NIR Raman spectra of the powdered samples were recorded on a Bruker RFS100/S spectrometer using near-infrared laser excitation (Nd: YAG, 785 nm). Factor group analysis based on above site symmetries predicted six Raman-active modes and the irreducible representations are given below.

$$\Gamma\,(\text{Raman}) = A_{1g} + E_g + 4F_{2g} \qquad [19, 20] \qquad (2)$$

Figure 3.3.1 shows the Raman spectrum of the $Gd_2Zr_2O_7$. $A_{1g}$, $E_g$ and $F_{2g}$ are Mullikan symbols representing different vibrational modes of the molecule, and the '+' symbol here merely represents combination of Raman-active vibrations. The $E_g$ (~327 $cm^{-1}$) mode can be assigned to B–O6 bending vibrations and the $A_{1g}$ (~541 $cm^{-1}$) mode to O–B–O bending vibrations. $F_{2g}$ (~248 $cm^{-1}$ and 554 $cm^{-1}$)modes represent a mixture of A–O and B–O bond stretching vibrations with bending vibrations and only one $F_{2g}$ (~410 $cm^{-1}$) mode relative to O-A-O'. According to factor group analysis, the only Raman-active mode of the fluorite-type structure is $F_{2g}$,

but in defect fluorites, the intensity of the $F_{2g}$ mode (554 $cm^{-1}$) is observed to be very weak, and appears as a broad peak[19, 20].

Since all the Raman active vibrations involve oxygen motion, the origin of broadening is mainly due to structural disorder present in the system due to structural vacancy from the statistical nature of the occupancy among various sites. The presence of vacancies and defects disrupts the translational periodicity of the lattice and consequently it relaxes the k = 0 selection rule. This may lead to the presence of additional modes, but of much lower intensity in Raman spectra. Other $F_{2g}$ bands are very weak in intensity and indistinguishable from the background. There is a progressive decrease in intensity of $A_{1g}$, $E_g$ and $F_{2g}$ modes, indicating a progressive disordering of the anion sublattice. For $x_{48f}$ values closer to the perfect pyrochlore phase ($0.309 \leq x_{48f} \leq 0.355$) the width is less and as the $x_{48f}$ parameter increases the width increases. This is directly related to the cationic antisite disorder leading to the oxygen disorder, which increases the width of the Raman lines[21]. A quantitative analysis of extent of disordering is not possible because of the weak intensity of the Raman peaks, but it confirms the results obtained from Rietveld analysis.

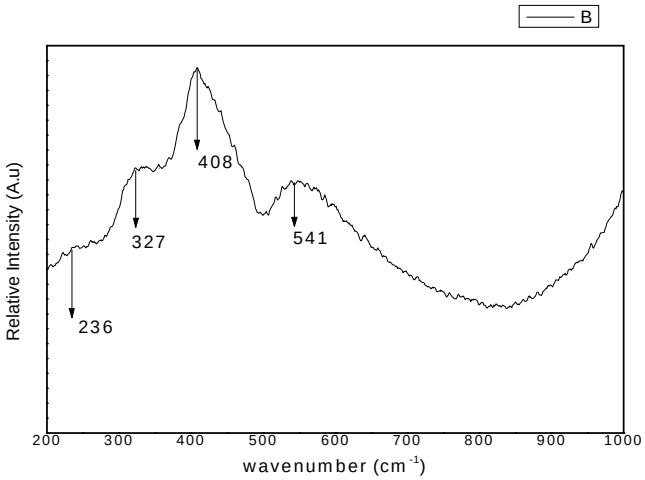


Figure 3.3.1 Raman spectrum of the $Gd_2Zr_2O_7$

*3.4 Determination of Band gap energy from UV-Visible Absorption Spectra :*

Figure 3.4.1 shows the UV–Vis transmittance spectra of the $Gd_2Zr_2O_7$ nanoceramics. The UV-Visible spectra of samples were recorded by dispersing the sample in ethanol medium using an ultrasonic bath. The absorption spectra were recorded at room temperature using SHIMADZU -2550 UV-Visible Spectrophotometer in the range from 200-800 nm. The absorption coefûcient near the fundamental edge depends on the photon energy and obeys the Tauc equation. According to Tauc's relation, the absorption coefficient a for direct-bandgap materials is given by

$$\alpha h\upsilon = A( h\upsilon - E_g )^n \quad (3)$$

where A is an energy-independent constant, α is the Kubelka–Munk (K–M) function and n is an index that depends on the nature of the electronic transition responsible for the optical absorption. The value of n for allowed direct transitions is ½ [22]. Figure 3.4.1 shows a Tauc plot of the optical absorption spectra at room temperature. The optical transition of the sample is reported to be an allowed direct one. Hence in the following analysis the value of n is set as 1/2. Figures 3.4.2 shows the plot of $(\alpha h\upsilon)^2$ versus $h\upsilon$ for sample. By extrapolating

the straight line portions of the plots, the exact value of the band gap are obtained and was found to be 4.82 eV [23].

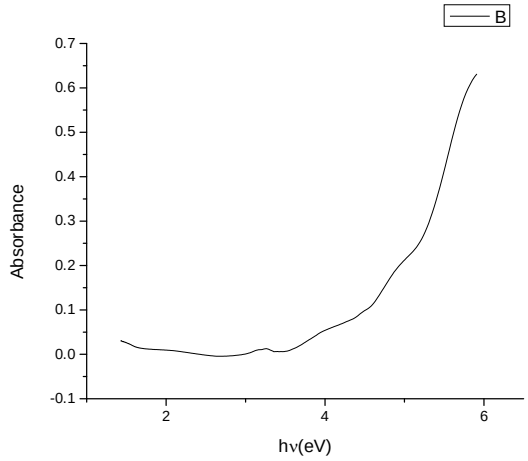


Figure 3.4.1The UV-Visible spectrum of the $Gd_2Zr_2O_7$

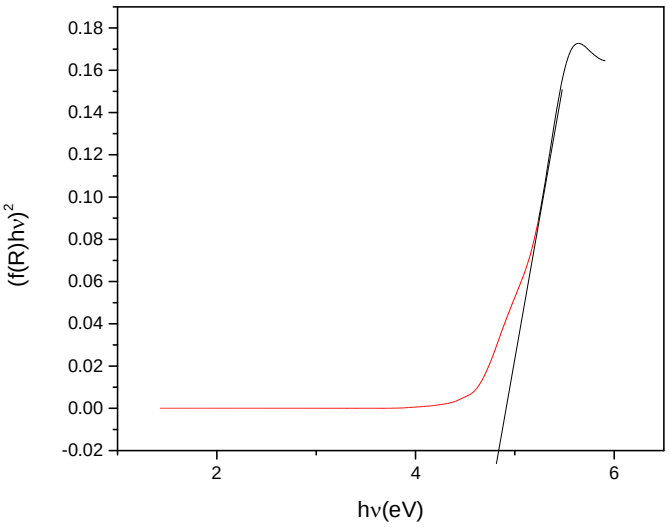


Figure 3.4.2: $(\alpha h\nu)^{1/n}$ versus hν plot for $Gd_2Zr_2O_7$

**3.5 Conclusion**

$Gd_2Zr_2O_7$ powders, synthesised by Solution combustion synthesis, were investigated in detail for the defect fluorite-pyrochlore phase transition behaviour at 1000°C. Our Xrd and Raman analyses clearly reveal the structural phase transition in this system. X-ray diffraction data analyses confirm that there is a defect fluorite structure in $Gd_2Zr_2O_7$ , having cubic lattice. The size difference between the cation species that occupy the A and B sites is believed to be the driving force for ordering in the Pyrochlore superstructure. Indeed, substituting a larger tetravalent cation in solid solution in the B site or a smaller trivalent cation in the A site progressively drives the structure to a disordered state in several systems, but not in cases where there is a strong covalent component to the bonding. Similar disordering behavior is found when the phases are heated. Thus, we believe

that the rearrangement in anionic sublattice in this system during structural phase transition from the Pyrochlore phase to disordered fluorite results in the shift in Pyrochlore-related peak. The decrease in value of $r_A/r_B$ ratio causes the distinction between A and B sites reduces; which further drives to form antisite defects and this causes local oxygen disorder which is evidenced by increased width of the Raman modes. Bandgap energy of the sample was obtained from UV-Visible spectroscopic analysis of the sample. It was found to be 4.82 eV.

### 3.6 References

1. P. M. van Dijk, K. J. deVries, and A. J. Burggraaf, Solid State Ionics 9/10, 913 (1983).
2. M.A. Subramanian, G. Aravamudan, G.V SubbaRao, Prog. Solid State Chem. 15, 55 (1983).
3. J. Wang, A. Nakamura, and M. Takeda, Solid State Ionics 164, 185 (2003).
4. T. Moriga, A. Yoshiasa, F. Kanamaru, K. Koto, M. Yoshimura, and S. Somiya, Solid State Ionics 31, 319 (1989).
5. R. C. Ewing, W. Weber, and J. Lian, *J. Appl. Phys. 95*, 5949 (2004).
6. B. P. Mandal and A. K. Tyagi. J. Alloys & Comps. 437, 260 (2007).
7. Jan Kuneš, W. E. Pickett, Phys B: Cond. Matter, 378, 898 (2006) .
8. S. N. Achary, S. K. Sali, K. Kulkarni, P. S. R. Krishna, A. B. Shinde, A. K. Tyagi, Chem.Mater. 21, 5848 (2009).
9. K. C. Patil, S. T. Aruna, and S. Ekambaram, Curr. Opinion in Solid State and Mater. Sci., 2,158 (1997).
10. K. C. Patil, S. T. Aruna and T. Mimani, Curr. Opin. Solid State Mater. Sci., 7 (2002).
11. S. R. Jain, K. C. Adiga, and V. R. Pai Verneker, Combust. Flame, 40, 71 (1981).
12. T. Mimani and K. C. Patil, Mater. Phys. Mech., *4*, 134 (2001).
13. A. S. Prakash, A. M. A. Khadar, K. C. Patil and M. S. Hegde , Journal of Materials Synthesis and Processing, *10*, 135-141 (2002).
14. M. Deepa, P. Prabhakar Rao, A. N. Radhakrishnan, K. S. Sibi and P. Koshy, Mater. Res. Bull., *44*, 1481–1488 (2009).
15. K. S. Sibi, A. N. Radhakrishnan, M. Deepa, P. Prabhakar Rao and P. Koshy, Solid State Ionics, *180*, 1164–1172 (2009).
16. Wuensch, B. J.; Eberman, K. W.; Hereman, C.; Ku, E. M.; Onnerud, P.; Yeo, E. M. E.; Haile, S. M.; Statlick, J. K.; Jorgensen, J. D. Solid State Ionics, 129, 111 (2000).
17. A. N. Radhakrishnan, P. Prabhakar Rao, K. S. Mary Linsa, M. Deepa and Peter Koshy,Dalton Transations, *40*, 3839-3848 (2011).
18. Fuentes, A. F.; Boulahya, K.; Maczka, M.; Hanuza, J.; Amador, U. Solid State Sci., *7*, 343 (2005).
19. B.P. Mandal, P.S.R. Krishna, and A.K. Tyagi, J. Solid State Chem. 183, 41 (2010).
20. Moreno, K. J.; Fuentes, A. F.; Maczka, M.; Hanuza, J.; Amador, U.; Santamaria, J.; Leon, C. Phys. ReV. B *75*, 184303 (2007).
21. J. Lian, J. Chen, L.M. Wang, R.C. Ewing, J.M. Farmer, L.A. Boatner, K.B. Helean, Phys. Rev. B 68, 134107 (2003).
22. A.S. Deepa, S. Vidya, P.C. Manu, S. Solomon, A. John, and J.K. Thomas, J. Alloys Compd. 509, 1830 (2011).
23. Sam Solomon, Aneesh George, Jijimon Kumpakkattu Thomas and Annamma John, Journal of Electronic Materials, Vol. *44*, No. 1, 28-37 (2015).